

## Broadband X-ray Spectral Analysis of the Dual AGN System Mrk 739

KOKI INABA <sup>1</sup>, YOSHIHIRO UEDA <sup>1</sup>, SATOSHI YAMADA <sup>2,1</sup>, SHOJI OGAWA <sup>1</sup>, RYOSUKE UEMATSU <sup>1</sup>,  
ATSUSHI TANIMOTO <sup>3</sup>, AND CLAUDIO RICCI <sup>4,5</sup>

<sup>1</sup>*Department of Astronomy, Kyoto University, Kitashirakawa-Oiwake-cho, Sakyo-ku, Kyoto 606-8502, Japan*

<sup>2</sup>*Institute of Physical and Chemical Research (RIKEN), 2-1 Hirosawa, Wako, Saitama 351-0198, Japan*

<sup>3</sup>*Graduate School of Science and Engineering, Kagoshima University, Kagoshima 890-0065, Japan*

<sup>4</sup>*Núcleo de Astronomía de la Facultad de Ingeniería, Universidad Diego Portales, Av. Ejército Libertador 441, Santiago, Chile*

<sup>5</sup>*Kavli Institute for Astronomy and Astrophysics, Peking University, Beijing 100871, People's Republic of China*

### ABSTRACT

We present the result of a broadband (0.5–70 keV) X-ray spectral analysis of the late-merger galaxy Mrk 739, which contains a dual active galactic nucleus (AGN), Mrk 739E and Mrk 739W, with a separation of 3.4 kpc. The spectra obtained with NuSTAR, Chandra, XMM-Newton and Swift/BAT are simultaneously analyzed by separating the contributions from the two AGNs and extended emission with the Chandra data. To evaluate the reflection components from the AGN tori, we consider two models, a phenomenological one (pexrav and zgauss) and a more physically motivated one (XCLUMPY; Tanimoto et al. 2019). On the basis of the results with XCLUMPY, we find that the AGNs in Mrk 739E and Mrk 739W have intrinsic 2–10 keV luminosities of  $1.0 \times 10^{43}$  and  $7.5 \times 10^{41}$  erg s<sup>-1</sup> absorbed by hydrogen column densities of  $N_{\text{H}} < 6.5 \times 10^{19}$  cm<sup>-2</sup> and  $N_{\text{H}} = 6.9_{-1.7}^{+3.2} \times 10^{21}$  cm<sup>-2</sup>, respectively. The torus covering fraction of the material with  $N_{\text{H}} > 10^{22}$  cm<sup>-2</sup> in Mrk 739E,  $C_{\text{T}}^{(22)} < 0.50$  at a 90% confidence limit, is found to be smaller than those found for late-merger ultra/luminous infrared galaxies,  $C_{\text{T}}^{(22)} = 0.71 \pm 0.16$  (mean and standard deviation; Yamada et al. 2021). Considering the small star formation rate of Mrk 739E, we suggest that the gas-to-mass ratio of the host galaxy is an important parameter to determine the circumnuclear environment of an AGN in late merger.

*Keywords:* Active galactic nuclei (16); Astrophysical black holes (98); High energy astrophysics (739); Supermassive black holes (1663); X-ray active galactic nuclei (2035)

### 1. INTRODUCTION

Past research since late 1990s has revealed that the masses of supermassive black holes (SMBHs) in galactic centers and those of galactic bulges are tightly correlated (e.g., Magorrian et al. 1998; Ferrarese & Merritt 2000; Kormendy & Ho 2013). These results imply that SMBHs and host galaxies have “coevolved” by regulating their respective growths. Galaxy mergers are thought to be one of the key paths to explain this coevolution, because they can facilitate both intense star formation in the nuclei and efficient mass accretion onto the SMBHs (e.g., Hopkins et al. 2008). Physical processes in the nuclear regions of merging galaxies are however poorly understood. Hence, investigating the circumnuclear environments of active galactic nuclei (AGNs) in galaxy mergers is crucial to elucidate the origin of the SMBH-galaxy coevolution.

Broadband X-ray observations are a powerful tool to study the structure of AGNs because X-rays are tracers of all material including gas and dust with various physical conditions. A key component to understand the AGN feeding mechanism is the so-called “torus” (e.g., Urry & Padovani 1995; Ramos Almeida & Ricci 2017), which is considered as the fuel reservoir of the SMBH. The spectral signatures of the X-ray radiation absorbed and/or reprocessed by the torus can provide constraints on its covering fraction and column density (e.g., Kawamuro et al. 2016; Tanimoto et al. 2020; Toba et al. 2020; Uematsu et al. 2021; Tanimoto et al. 2022).

Recently, Yamada et al. (2021) have conducted a systematic X-ray study of AGNs in 57 local ultra/luminous

infrared galaxy (U/LIRG) systems<sup>1</sup>, most of which are identified to be merging galaxies. They find that the AGNs in merging U/LIRG systems become more deeply “buried” (i.e., covered by matter with a large solid angle) with merging stage, confirming the implication by Ricci et al. (2017a, 2021) based on the absorption column-density distribution of local mergers (see also Imanishi et al. 2006, 2008; Yamada et al. 2019). In particular, it is found that AGNs in late-stage mergers with high Eddington ratios ( $\log \lambda_{\text{Edd}} > -1.5$ ) show larger torus covering fractions than those in nonmergers. These results are in line with the theoretical prediction that a galaxy merger triggers rapid mass accretion deeply embedded by gas and dust (e.g., Hopkins et al. 2006; Blecha et al. 2018; Kawaguchi et al. 2020). However, since their sample is limited to U/LIRG populations, which have high star formation rates (SFRs), the relation of the “buried AGN” nature with the host properties (e.g., star-formation rate, gas mass, stellar mass) remains unclear.

To test if galaxy mergers commonly produce AGNs with large covering fractions regardless of their SFRs, here we focus on the AGNs in a late-stage merging galaxy that is *less luminous* in the infrared band than U/LIRGs. We choose Mrk 739 ( $z = 0.0297$ ) as our target. It is a merging system consisting of Mrk 739E and Mrk 739W with a projected separation of  $\approx 3.4$  kpc, the second smallest value among the Swift/BAT dual-AGN sample by Koss et al. (2012). This defines this system as a late-stage (stage C) merger according to the criteria of Stierwalt et al. (2013). However, unlike many other late-stage mergers, Mrk 739 is not infrared luminous ( $L_{\text{IR}} \sim 10^{10.9} L_{\odot}$ ; e.g., Imanishi & Saito 2014) enough to be categorized as a LIRG, and hence is not included in the sample of Yamada et al. (2021). The optical spectrum of Mrk 739E shows broad emission lines, identifying it as a type-1 AGN (Netzer et al. 1987, Koss et al. 2011, Tubín et al. 2021). Koss et al. (2011) suggest that Mrk 739W also contains an AGN on the basis of the hard photon index in the soft X-ray (0.5–10 keV) band. The optical spectra of Mrk 739W show no evidence for broad emission lines, which may be contaminated by strong starburst components (Tubín et al. 2021).

In this work, we aim to answer the question whether or not the AGN tori in the Mrk 739 system have large covering fractions. For this purpose, we conduct a broadband (0.5–70 keV) X-ray spectral analysis of Mrk 739, utilizing the currently best available dataset

obtained with NuSTAR, Chandra, XMM-Newton, and Swift/BAT. The NuSTAR data of Mrk 739 are presented here for the first time.

The paper is organized as follows. In Section 2, we describe the observations and reduction of the data obtained with the four satellites. Section 3 describes the X-ray spectral model and give the results of spectral fitting. To constrain the torus structure by assuming realistic geometry, we apply an X-ray clumpy torus model (XCLUMPY; Tanimoto et al. 2019), which was also adopted in Yamada et al. (2021). Finally, we discuss the properties of the AGN of Mrk 739E, which is  $\sim 15$  times brighter than that of Mrk 739W, mainly focusing on its torus structure in Section 4. Section 5 reports the conclusions of this work. In this paper, we assume the solar abundances by Anders & Grevesse (1989). Throughout this paper, we adopt the cosmological parameters of  $H_0 = 70 \text{ km s}^{-1} \text{ Mpc}^{-1}$ ,  $\Omega_{\text{M}} = 0.3$ , and  $\Omega_{\Lambda} = 0.7$ . Errors on spectral parameters correspond to 90% confidence limits for a single parameter of interest.

## 2. OBSERVATIONS AND DATA REDUCTION

The observation log of the X-ray spectral data used in this paper (NuSTAR, Chandra, XMM-Newton, and Swift/BAT) is summarized in Table 1. We conducted data reduction in accordance with the procedures described below.

### 2.1. NuSTAR

NuSTAR (Harrison et al. 2013) observed Mrk 739 with the two focal plane modules (FPMs: FPMA and FPMB), which are sensitive to X-ray energies in the 3–79 keV band. The observation was performed on 2017 March 16 for an exposure time of 18.5 ks. The data presented here were reduced by using HEASoft v6.28 and CALDB v20201217. FPMs’ data were reprocessed by using NUPIPELINE and NUPRODUCTS.

We extracted spectral data from a circular region with a radius of  $60''$ , and subtracted the background taken from an annulus with inner and outer radii of  $60''$  and  $120''$  surrounding the source concentrically. Considering the limited photon statistics, we coadded the source spectra, background spectra, RMF, and ARF of the two FPMs by using ADDASCASPEC. We grouped bins so that each of them included at least 50 photon counts. The angular resolution of NuSTAR is  $58''$  in full width at half maximum (FWHM), which is not sufficient to separate the AGNs in the two galaxies (Mrk 739E and Mrk 739W) of the system. Hence, our NuSTAR spectrum contains emission from both AGNs and galaxies.

### 2.2. Chandra

<sup>1</sup> Those with infrared (8–1000  $\mu\text{m}$ ) luminosities of  $L_{\text{IR}} \geq 10^{12} L_{\odot}$  and of  $L_{\text{IR}} = 10^{11} - 10^{12} L_{\odot}$  are called ULIRGs and LIRGs, respectively (Sanders & Mirabel 1996).

Chandra (Weisskopf et al. 2002) observed Mrk 739 with the Advanced CCD Imaging Spectrometer (ACIS: Garmire et al. 2003). The observation was performed on 2011 April 22 for an exposure time of 13.0 ks. The data were reduced in the standard manner using the Chandra Interactive Analysis of Observations (CIAO v4.12) software and calibration files (CALDB v4.9.2.1). Thanks to its good angular resolution ( $<1''$ ), Chandra was able to spatially resolve the two galaxies and the extended soft X-ray emission surrounding them (Koss et al. 2011).

Thus, we extracted three spectral regions: two circular regions with radii of  $3''$  and  $2''$ , respectively, centered on the galactic centers of Mrk 739E and Mrk 739W. For the extended emission, we adopt a circular region with a radius of  $10''$  from which the two circular regions mentioned above were excluded (see Figure 1). Additionally, we excluded a rectangle region ( $2'' \times 10''$ ) where instrumental noises are prominent. We subtracted the background, which was taken from a source-free circular region with a radius of  $10''$  on the same chip. We grouped bins of the spectra of Mrk 739E, Mrk 739W, and the soft extended emission, respectively, so that each bin included at least 20 photon counts.

### 2.3. XMM-Newton

XMM-Newton (Jansen et al. 2001) observed Mrk 739 on 2009 June 14 for an exposure time of 11.9 ks with the European Photon Imaging Cameras (EPICs). We reduced the data with the science analysis software (SAS) v18.0.0 and current calibration files (CCF) released on 2020 May 14. In this paper, we only utilized the data of pn (Strüder et al. 2001), which has larger effective area than MOS1 and MOS2.

The angular resolution of XMM-Newton,  $15''$  (FWHM), is not small enough to separate the two galactic centers of Mrk 739. Thus, we extracted spectral data from a single circular region with a radius of  $40''$ . The background was taken from a circular source-free region with a radius of  $40''$  on the same chip. We grouped bins of source so that at least 50 photon counts were included per bin.

### 2.4. Swift/BAT

We also utilized the hard X-ray spectrum of Mrk 739 obtained with Burst Alert Telescope (BAT) on the Neil Gehrels Swift observatory (Gehrels et al. 2004) averaged over 105 months (Oh et al. 2018) from 2004 December to 2013 August.

To best constrain the properties of the AGNs, we take the same approach as adopted by Yamada et al. (2018) for the local merging galaxy Mrk 463. We perform simultaneous fit to the six spectra: the individual spectra of Mrk 739E, Mrk 739W, and the extended emission observed with Chandra/ACIS-S (in the 0.5–7.0 keV, 0.8–5.0 keV, 0.5–3.0 keV bands, respectively), and the total spectra from the whole Mrk 739 system observed with NuSTAR/FPMs (3.0–60 keV), XMM-Newton/pn (0.5–10 keV), and Swift/BAT (20–70 keV). Here we adopt the energy intervals where the spectra have sufficiently high signal-to-noise ratios. Spectral fitting is performed on XSPEC (Arnaud 1996) v12.11.1 based on  $\chi^2$ -statistics. We always consider the Galactic absorption (total of H I and H<sub>2</sub>), whose hydrogen column density is fixed at  $2.14 \times 10^{20} \text{ cm}^{-2}$  (Willingale et al. 2013).

## 3.1. AGN Spectral Model

In this section, we describe the details of spectral models for the AGNs in Mrk 739E and Mrk 739W. We first begin with a simple phenomenological model (Model I). Then, we apply a more physically motivated one (Model II) to constrain the torus parameters.

### 3.1.1. Model I

A typical X-ray spectrum of an AGN (e.g., Ogawa et al. 2019) consists of a direct component, which is often subject to absorption by line of sight matter (e.g., warm absorbers, torus), reflected components from the torus and/or the accretion disk accompanied by fluorescence lines, and a Thomson-scattered component (plus emission from a photoionized plasma). In addition to the AGN emission, optically-thin thermal emission from the host galaxy is often present.

Thus, we consider these AGN components for the Mrk 739E and Mrk 739W spectra except for Thomson-scattered ones, which are not significantly required in our data. Firstly, we perform spectral fitting without any reflection components. We find, however, that the model systematically underproduces the hard X-ray flux above 10 keV by a factor of 2, suggesting the presence of a reflection hump by the torus and/or the accretion disk in Mrk 739. We also see a hint of a narrow emission line around 6.4 keV in the XMM-Newton spectrum. Accordingly, we add the pexrav (Magdziarz & Zdziarski 1995) and zgauss components to represent the reflection continua from cold matter and Fe K $\alpha$  fluorescence lines, respectively. The models for Mrk 739E and Mrk 739W are expressed as follows in XSPEC terminology:

$$\begin{aligned} \text{Mrk 739E} &= \text{const0*phabs} \\ & * (\text{const1*zphabs*cabs} \end{aligned}$$

## 3. X-RAY SPECTRAL ANALYSIS

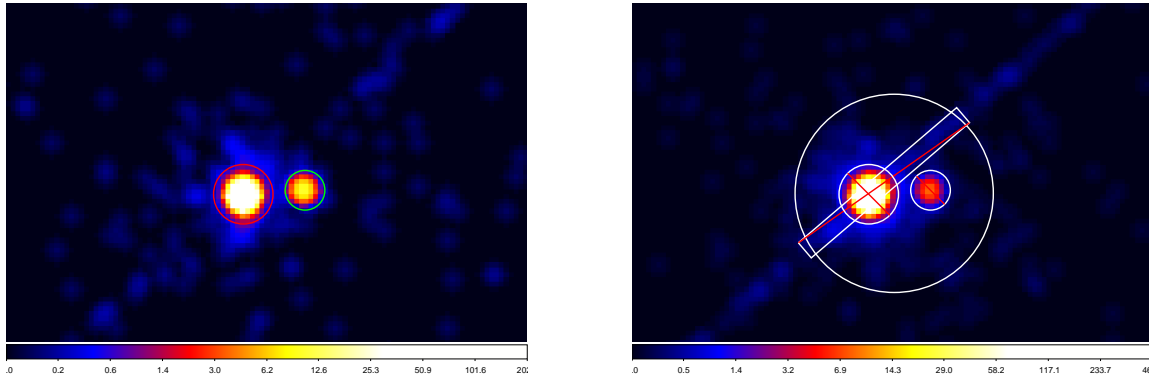


**Figure 1.** (Left) Chandra/ACIS-S image of the central region of the Mrk 739 system in the 2.0-8.0 keV band, smoothed with a 2D Gaussian of a  $\sigma$  radius of 1.5 pixels (each pixel is  $0.492''$ ). The spectral extraction regions for Mrk 739E and Mrk 739W are marked by the left (red) and right (green) circles, respectively. (Right) The same but in the 0.4-2.0 keV band. The large circle (white) marks the the spectral region for the extended emission from which the rectangle region containing a readout streak and the two circular regions in the left panel are excluded.

**Table 1.** Summary of Observations

Satellite	ObsID	Start Date (UT)	End Date (UT)	Net exposure (ks) <sup>a</sup>
NuSTAR	60260008002	2017-03-16 03:56:09	2017-03-16 09:05:16	18.5
Chandra (ASIS-S)	12863	2011-04-22 02:26:55	2011-04-22 06:03:45	13.0
XMM-Newton	0601780401	2009-06-14 08:23:45	2009-06-14 11:42:21	11.9
Swift/BAT	-	2004 December	2013 August	-

<sup>a</sup>Based on the good time interval of FPMA for NuSTAR and EPIC-pn for XMM-Newton.

$$\begin{aligned}
 & * \text{mtable}\{\text{xout\_mtable.fits}\} \\
 & * \text{zcutoffpl} \\
 & + \text{pexrav} + \text{zgauss} \\
 & + \text{apec}
 \end{aligned} \tag{1}$$

$$\begin{aligned}
 \text{Mrk 739W} = & \text{const0} * \text{phabs} \\
 & * (\text{const1} * \text{zphabs} * \text{cabs} \\
 & * \text{zcutoffpl} \\
 & + \text{pexrav} + \text{zgauss})
 \end{aligned} \tag{2}$$

- (1) The `const0` and `phabs` terms represent the cross calibration factor of among different instruments and the Galactic absorption, respectively. We set `const0` of NuSTAR to unity as the reference. We also fix that of Swift/BAT at unity, which would be strongly coupled with `const1` otherwise. Those of Chandra and XMM-Newton are set to the values derived by Madsen et al. (2017), 1.09 and 0.89, considering the limited photon statistics.
- (2) The `const1` factor takes into account time variability of Mrk 739E among different observational

epochs. We ignore time variability of Mrk 739W (i.e., `const1` is set to unity) because the flux of Mrk 739W is too faint to detect any variability. To confirm the validity of this assumption, we also perform spectral fitting by adopting the `const1` values of 0.3 or 3.0 (a typical variability range of nearby AGNs over  $\sim 10$  years; Kawamuro et al. 2016) for Chandra, XMM-Newton, and Swift/BAT data. Except for the two cases where the  $\chi^2$  values are unacceptably increased by  $\gtrsim 30$ , we find that the choices of `const1` values do not affect our main conclusion. The `zphabs` and `cabs` terms represent photoelectric absorption and Compton scattering, respectively. The hydrogen column density along the line of sight is fixed at  $N_{\text{H}}^{\text{LOS}} = 10^{19} \text{ cm}^{-2}$  (the best-fit value obtained with Model II, see Section 3.3.2.), which cannot be well constrained with Model I.

- (3) The multiplicative table model `mtable}\{\text{xout\_mtable.fits}\}` represents absorptions by ionized matter, often called “warm absorbers”. To generate the table model, we utilized XSTAR v2.54a (Kallman & Bautista 2001; Bautista &

Kallman 2001) assuming the solar abundances. We assume that the ionization parameter ( $\xi$ ) and hydrogen column density ( $N_{\text{H}}$ ) are variable among different epochs. Since NuSTAR does not cover the soft X-ray band, we adopt the same parameters as determined by the Chandra data for the NuSTAR spectrum.

- (4) The `zcutoffpl` term is a direct component (a power-law with an exponential high energy cutoff). Here, we assume that the power-law photon index did not vary during the different observational epochs. The cutoff energy is fixed at 160 keV as a typical value of AGNs (Ricci et al. 2018). The `pexrav` term represents a reflection component from optically-thick cold matter (Magdziarz & Zdziarski 1995). `pexrav` has eight parameters, the power law photon index ( $\Gamma$ ), the cutoff energy ( $E_{\text{cut}}$ ), the reflection strength ( $R \equiv \Omega/2\pi$ , where  $\Omega$  is the solid angle of the reflector), the redshift ( $z$ ), the abundance ( $Z$ ; elements heavier than He), the iron abundance ( $Z_{\text{Fe}}$ ), the inclination angle ( $i$ ), and the normalization ( $K_{\text{ref}}$ ). We link  $\Gamma$ ,  $E_{\text{cut}}$ , and  $K_{\text{ref}}$  to those of the direct component. We assume that  $Z = 1$  and  $Z_{\text{Fe}} = 1$  (i.e., solar abundances). The inclinations of Mrk 739E and Mrk 739W are fixed at  $i = 45^\circ$  and  $i = 60^\circ$ , respectively (see the description of Model II component (5) in Equation (3)). We set  $R$  of Mrk 739E to be free within a negative range ( $-2 \leq R \leq 0$ ) to obtain only the reflected component. Due to the limited photon statistics, we fix  $R$  of Mrk 739W at  $-0.8$ , the average value for nearby moderately-obscured AGNs (Kawamuro et al. 2016). The `zgauss` term represents an Fe  $K\alpha$  fluorescence line, whose center energy and  $1\sigma$  width are fixed at 6.4 keV and of 20 eV, respectively. While we set the normalization of Mrk 739E to be free, we fix that of Mrk 739W so that the Fe  $K\alpha$  lines of the two AGNs have similar equivalent widths with respect to the `pexrav` components.
- (5) The last term, `apec`, represents optically-thin thermal plasma due to the star formation activity in the host galaxy. We assume the parameters to be invariable among different epochs.

In the spectral model of Mrk 739W, we do not include the warm-absorber and optically-thin thermal plasma, which are not significantly required from our spectra. The analysis results with Model I are mentioned in Section 3.3.

### 3.1.2. Model II

As a more physically motivated model, we replace the torus reflection component `pexrav` and `zgauss` in Model I with the X-ray clumpy torus model XCLUMPY (Tanimoto et al. 2019). This enables us to constrain the torus structure and to compare our results with those of AGNs in late mergers obtained by Yamada et al. (2021).

We find, however, that a hard X-ray excess around 20 keV remains with this model. This is because XCLUMPY whose parameters are mainly constrained by the line-of-sight absorption and the narrow Fe  $K\alpha$  equivalent width produces a much weaker hard X-ray reflection hump than the `pexrav` component in Model I. This suggests the presence of a relativistically blurred reflection component from the accretion disk that produces a strong reflection hump at  $\sim 20$  keV but not a “narrow” Fe  $K\alpha$  line (see also Section 3.3). Accordingly, we added a `relxill` component for Mrk 739E. The final spectral models of Mrk 739E and Mrk 739W are expressed as follows in XSPEC terminology:

$$\begin{aligned}
 \text{Mrk 739E} = & \text{const0*phabs} \\
 & * (\text{const1*zphabs*cabs} \\
 & * \text{mtable}\{\text{xout\_mtable.fits}\} \\
 & * (\text{zcutoffpl} + \text{relxill}) \\
 & + \text{atable}\{\text{xclumpy\_v01\_RC.fits}\} \\
 & + \text{atable}\{\text{xclumpy\_v01\_RL.fits}\} \\
 & + \text{apec}
 \end{aligned} \tag{3}$$

$$\begin{aligned}
 \text{Mrk 739W} = & \text{const0*phabs} \\
 & * (\text{const1*zphabs*cabs} \\
 & * \text{zcutoffpl} \\
 & + \text{atable}\{\text{xclumpy\_v01\_RC.fits}\} \\
 & + \text{atable}\{\text{xclumpy\_v01\_RL.fits}\}
 \end{aligned} \tag{4}$$

- (1) Same as the component (1) of Equation (1).
- (2) Same as the component (2) of Equation (1). Here, the hydrogen column density along the line of sight is not a free parameter, but determined by the torus parameter (see Equation 5).
- (3) Same as the component (3) of Equation (1).
- (4) Same as the component (4) of Equation (1) in terms of `zcutoffpl`. The `relxill` term represents a relativistic reflection component from the accretion disk (Dauser et al. 2013; García et al. 2014). This model (RELXILL) combines the XILLVER code (García et al. 2014), which calculates a reflected spectrum from the accretion disk, and the

RELLINE code (Dauser et al. 2010, 2013), which takes into account relativistic smearing effects. RELXILL has 14 parameters: the inner ( $R_{\text{in}}$ ) and outer ( $R_{\text{out}}$ ) radii of the disk, the boundary radius ( $R_{\text{br}}$ ) at which the emissivity index changes, the index ( $q_1$ ) which gives emissivity as  $r^{-q_1}$  between  $R_{\text{in}}$  and  $R_{\text{br}}$ , the index ( $q_2$ ) which gives emissivity as  $r^{-q_2}$  between  $R_{\text{br}}$  and  $R_{\text{out}}$ , the spin parameter of the black hole ( $a$ ), the inclination angle ( $i$ ) between the line of sight and the line perpendicular to the disk, the redshift ( $z$ ), the power-law index ( $\Gamma$ ), the ionization parameter of the disk ( $\xi$ ), the iron abundance ( $Z_{\text{Fe}}$ ), the cutoff energy ( $E_{\text{cut}}$ ), the ratio ( $R$ ) of the solid angle of the reflector to  $2\pi^2$ , and the normalization ( $K_{\text{rel}}$ ). The photon index ( $\Gamma$ ) and cutoff energy ( $E_{\text{cut}}$ ) are linked between the direct component and RELXILL. The inclination angle ( $i$ ) is fixed at the same value as in the `pextrav` model (see the component (5)). We assume that  $R_{\text{in}} = R_{\text{ISCO}}$ ,  $R_{\text{out}} = 10^3 r_g$  ( $r_g$  is the gravitational radius),  $q_1 = q_2 = 2.4$ , which is a mean value for local Seyfert 1 galaxies (Patrick et al. 2012),  $a = 0$ ,  $\xi = 0$ , and  $Z_{\text{Fe}} = 1.0$  (i.e., solar abundances), because these parameters cannot be well constrained by our data. We set  $R = -0.25$  to obtain only the reflected component. Thus, the free parameter of RELXILL in our fitting is only the normalization ( $K_{\text{rel}}$ ). Since both `zcutoffpl` and `relxill` components are emitted from a compact region much smaller than light years, we assume that they are subject to the same absorption and time variability factor (`const1`).

- (5) The `atable{xclumpy_v01_RC.fits}` and `atable{xclumpy_v01_RL.fits}` term correspond to the reflection continuum and fluorescence lines from the torus, respectively, based on the XCLUMPY model (Tanimoto et al. 2019). The parameters of XCLUMPY are the hydrogen column density along the equatorial plane ( $N_{\text{H}}^{\text{Equ}}$ ), the torus angular width ( $\sigma$ ), the inclination angle ( $i$ ), the power-law photon index ( $\Gamma$ ), the cutoff energy ( $E_{\text{cut}}$ ), the redshift ( $z$ ), and the normalization ( $K_{\text{ref}}$ ). We link  $\Gamma$ ,  $E_{\text{cut}}$ , and  $K_{\text{ref}}$  to those of the direct component. The inclination of Mrk 739E is fixed at  $i = 45^\circ$ , a typical value for Seyfert 1 galaxies as constrained by the XCLUMPY model (Ogawa et al. 2021). The inclination of Mrk 739W is fixed at  $i = 60^\circ$  because a lower  $i$  value makes

$N_{\text{H}}^{\text{Equ}}$  pegged at its upper boundary ( $10^{25} \text{ cm}^{-2}$ ). Thus, the free parameters are  $N_{\text{H}}^{\text{Equ}}$  and  $\sigma$ . Because of coupling between the two parameters, however, we find it difficult to determine both values simultaneously. Hence, we conduct three patterns of spectral fitting by fixing  $\sigma$  of Mrk 739E at  $10^\circ$ ,  $15^\circ$ , or  $20^\circ$ <sup>3</sup>. The torus angular width  $\sigma$  of Mrk 739W is fixed at  $15^\circ$ , which cannot be well constrained. From  $N_{\text{H}}^{\text{Equ}}$  and  $\sigma$ , the hydrogen column density along the line of sight ( $N_{\text{H}}^{\text{LOS}}$ ) at the elevation angle  $\theta$  ( $= 90^\circ - i$ ) is calculated as follows:

$$N_{\text{H}}^{\text{LOS}}(\theta) = N_{\text{H}}^{\text{Equ}} \exp\left(-\left(\frac{\theta}{\sigma}\right)^2\right). \quad (5)$$

This value of  $N_{\text{H}}^{\text{LOS}}(\theta)$  is applied to the absorption terms in (2). Considering that the large size of the torus ( $\sim \text{pc}$ ), we assume that the flux of the torus reflection component is invariable among the different observation epochs, which were separated by 2–8 years.

- (6) Same as the component (5) of Equation (1).

The analysis results with Model II are mentioned in Section 3.3.2.

### 3.2. Extended Emission

Generally, extended emission around an AGN consists of scattered/photoionized component from the AGN and optically-thin thermal emission from the host galaxy. Since we find that thermal emission modelled by `apec` is not required by our data, we employ only a simple power-law as the scattered AGN component. The final model of the extended emission is expressed as follows in XSPEC terminology:

$$\text{Extended} = \text{const0} * \text{phabs} * \text{zcutoffpl} \quad (6)$$

- (1) Same as Mrk 739E component (1).  
 (2) The `zcutoffpl` term represents scattered components from the AGNs in Mrk 739E and Mrk 739W. This component is assumed to be constant over all the observations. We correct for the effect of excluding the rectangle area in the spectral extraction region of the Chandra spectrum by assuming a constant surface brightness.

<sup>2</sup> When this parameter is set to a negative value, only the reflected component is returned

<sup>3</sup> We note that  $\sigma = 10^\circ$  corresponds to the lower boundary of the parameter range in XCLUMPY, and adopting  $\sigma \geq 25^\circ$  makes  $N_{\text{H}}^{\text{Equ}}$  pegged at its lower boundary ( $10^{23} \text{ cm}^{-2}$ ).

### 3.3. Results

#### 3.3.1. Results-of-Model-I

The phenomenological model, Model I, is able to reproduce the observed spectra of the six instruments simultaneously. Table 2 (Model I) summarizes the best-fit parameters. In Mrk 739E, time-variable warm absorbers with  $\log N_{\text{H}}/\text{cm}^2 \sim (21.5\text{--}22.0)$  are detected. Line-of-sight absorption by neutral material with  $\log N_{\text{H}}/\text{cm}^2 = 21.9^{+0.19}_{-0.17}$  is required in Mrk 739W. An  $F$ -test verifies that the addition of the `pexrav` and `zgauss` components significantly improves the fit at a  $>99\%$  confidence level ( $\chi^2/\text{d.o.f} = 649.0/618$  from  $\chi^2/\text{d.o.f} = 679.9/620$ ). We obtain a reflection strength of  $R = -1.12^{+0.48}_{-0.66}$  and an equivalent width of a narrow Fe  $K\alpha$  line of  $55 \pm 46$  eV for Mrk 739E. We note that this equivalent width is smaller than the theoretical prediction from the observed `pexrav` component ( $\gtrsim 110$  eV) as estimated with the `pexmon` model (Nandra et al. 2007). This may support the presence of a relativistic reflection component introduced in Model II (Section 3.1.2).

#### 3.3.2. Results-of-Model-II

We find that Model II also well reproduces the data. Table 2 (Model II) summarizes the best-fit parameters for the case of  $\sigma = 15^\circ$ . The presence of the variable warm absorbers in Mrk 739E is confirmed. An  $F$ -test confirms that the addition of the `relxill` term provides a significantly better fit at a  $>99\%$  confidence level ( $\chi^2/\text{d.o.f} = 644.7/618$  from  $\chi^2/\text{d.o.f} = 665.4/619$ ). The observed spectra and the best-fit model are plotted in Figure 2 and Figure 3, respectively. As mentioned above, the main features in the observed spectra that constrain the torus parameters of XCLUMPY are the line of sight column density (or its upper limit) and the equivalent width of the Fe  $K\alpha$  line. As evident from Equation (5) and Equation (7) of this paper and Figure 3 of Ogawa et al. (2019), respectively, these constraints inevitably cause parameter coupling (anti correlation) between  $N_{\text{H}}^{\text{Equ}}$  and  $\sigma$ . To check if our main results would be affected by this, we also perform spectral fitting by fixing  $\sigma$  at  $10^\circ$  or  $20^\circ$  for Mrk 739E. We confirm that the spectra are also well reproduced. The best-fit values of  $N_{\text{H}}^{\text{Equ}}$  and reduced  $\chi^2$  values for the three cases ( $\sigma = 10^\circ, 15^\circ, 20^\circ$ ) are summarized in the Table 3.

## 4. DISCUSSION

### 4.1. Result Summary

We have analyzed the highest-quality available broadband X-ray spectra of the Mrk 739 system obtained with NuSTAR, Chandra, XMM-Newton, and Swift/BAT, covering the 0.5–70 keV band. Thanks to the superior angular resolution of Chandra, it is possible to separately analyze the spectra of three different regions, Mrk 739E, Mrk 739W, and the extended emission (Figure 1). We verify that the spectra of the other instruments can be reproduced with the sum of these three spectra by taking into account time variability in the flux of the direct components and warm-absorber parameters (for Mrk 739E). In particular, the NuSTAR data constrain well the broadband spectrum of the brighter AGN, Mrk 739E. To model the reflection components from the tori, we employ two models; `pexrav` (Model I, Magdziarz & Zdziarski 1995) and XCLUMPY (Model II, Tanimoto et al. 2019). Here, we mainly discuss the results obtained by Model II, where more realistic torus geometry is assumed.

Through this analysis, we are able to best constrain the X-ray properties of the two AGNs. We obtain the intrinsic 2–10 keV luminosities of  $1.0 \times 10^{43}$  and  $7.5 \times 10^{41}$  erg  $\text{s}^{-1}$  and absorption column densities by neutral material of  $N_{\text{H}} < 6.5 \times 10^{19}$   $\text{cm}^{-2}$  and  $N_{\text{H}} = 6.9^{+3.2}_{-1.7} \times 10^{21}$   $\text{cm}^{-2}$  for Mrk 739E and Mrk 739W, respectively, at the epoch of the Chandra observation in April 2011. These results are essentially consistent with the previous study using Chandra and Swift/BAT (Koss et al. 2011), except that the column density of Mrk 739E is smaller than their estimate because of the inclusion of the warm absorbers in our analysis. We confirm that Mrk 739E is an unabsorbed moderately-luminous AGN, whereas Mrk 739W is a weakly absorbed, low-luminosity AGN. In the following, we focus on the AGN properties of Mrk 739E, which is  $\sim 15$  times brighter than Mrk 739W in the 2–10 keV band.

### 4.2. AGN Properties of Mrk 739E

We examine whether the AGN torus in Mrk 739E has a larger covering fraction than those of “normal AGNs” (i.e., those in nonmergers or early-stage mergers) based on the results obtained by Model II. The torus covering fraction,  $C_{\text{T}}^{(22)}$  is defined as the solid angle of torus matter with column densities of  $\log N_{\text{H}}/\text{cm}^{-2} > 22$  normalized by  $4\pi$ . Using a Swift/BAT selected AGN sample, Ricci et al. (2017b) find that the Eddington ratio ( $\lambda_{\text{Edd}}$ ) is the key parameter that determines the torus structure;  $C_{\text{T}}^{(22)}$  rapidly decreases from  $\sim 0.8$  to  $\sim 0.3$  at  $\log \lambda_{\text{Edd}} > -1.5$ . This suggests that the AGN tori are regulated by radiation pressure on dusty gas within sphere of influence of the SMBH (see also Ricci et al. 2022). By contrast, as we mention in Section 1, Yamada

**Table 2.** Best-fit Spectral Parameters ( $\sigma = 15$ )

Region	Component	No.	Parameter	Model I	Model II	Units
Mrk 739E	mtable{xout_mtable.fits}	(1)	$N_{\text{H}}$	$8.57^{+1.02}_{-1.12}$ , $3.06^{+0.68}_{-0.62}$	$8.80^{+1.04}_{-1.01}$ , $3.79^{+0.81}_{-0.78}$	$10^{21} \text{ cm}^{-2}$
		(2)	$\log \xi$	$0.89^{+0.07}_{-0.09}$ , $0.58^{+0.09}_{-0.10}$	$0.74^{+0.07}_{-0.06}$ , $0.41^{+0.06}_{-0.17}$	
	zcutoffpl	(3)	$\Gamma_{\text{AGN}}$	$2.07^{+0.06}_{-0.05}$	$2.15^{+0.09}_{-0.06}$	
		(4)	$K_{\text{AGN}}$	$1.81^{+0.16}_{-0.15}$	$1.91^{+0.19}_{-0.15}$	$10^{-3} \text{ keV}^{-1} \text{ cm}^{-2} \text{ s}^{-1}$
	relxill	(5)	$K_{\text{RELXILL}}$	...	$5.25^{+2.92}_{-1.70}$	$10^{-5} \text{ keV}^{-1} \text{ cm}^{-2} \text{ s}^{-1}$
	pexrav	(6)	$R$	$-1.12^{+0.48}_{-0.66}$	...	
	zgauss	(7)	$K_{\text{Fe}}$	$2.66^{+2.22}_{-2.22}$	...	$10^{-6} \text{ keV}^{-1} \text{ cm}^{-2} \text{ s}^{-1}$
	atable{xclumpy_v01_RC(L).fits}	(8)	$N_{\text{H}}^{\text{Equ}}$	...	$< 5.30$	$10^{23} \text{ cm}^{-2}$
		(9)	$\sigma$	...	15.0 (fixed)	degree
	apec	(10)	$K_{\text{apec}}$	$1.29^{+0.26}_{-0.21}$	$1.40^{+0.42}_{-0.27}$	$10^{-4} \text{ cm}^{-5}$
		(11)	$k\text{T}$	$0.51^{+0.06}_{-0.08}$	$0.45^{+0.07}_{-0.09}$	keV
	const1	(12)	$N_{\text{Chandra}}$	$1.26^{+0.08}_{-0.07}$	$1.25^{+0.07}_{-0.07}$	
		(13)	$N_{\text{XMM}}$	$1.34^{+0.08}_{-0.07}$	$1.33^{+0.07}_{-0.07}$	
	---	(14)	$N_{\text{Swift/BAT}}$	$2.24^{+0.78}_{-0.75}$	$1.87^{+0.46}_{-0.43}$	
		(15)	$N_{\text{H}}^{\text{LOS}}$	1.00 (fixed)	$< 6.54$	$10^{19} \text{ cm}^{-2}$
		(16)	$L_{2-10,\text{E}}$	1.08	1.00	$10^{43} \text{ erg s}^{-1}$
Mrk 739W	zcutoffpl	(17)	$\Gamma_{\text{AGN}}$	$1.55^{+0.54}_{-0.05(*)}$	$1.50^{+0.40}_{-0.00(*)}$	
		(18)	$K_{\text{AGN}}$	$6.94^{+6.41}_{-1.31}$	$6.57^{+4.44}_{-0.95}$	$10^{-5} \text{ keV}^{-1} \text{ cm}^{-2} \text{ s}^{-1}$
	pexmon	(19)	$R$	-0.8 (fixed)	...	
	atable{xclumpy_v01_RC(L).fits}	(20)	$N_{\text{H}}^{\text{Equ}}$	...	$3.76^{+1.74}_{-0.95}$	$10^{23} \text{ cm}^{-2}$
		(21)	$N_{\text{H}}^{\text{LOS}}$	$7.26^{+4.48}_{-2.07}$	$6.89^{+3.18}_{-1.74}$	$10^{21} \text{ cm}^{-2}$
	---	(22)	$L_{2-10,\text{W}}$	7.32	7.46	$10^{41} \text{ erg s}^{-1}$
Extended	zcutoffpl	(23)	$\Gamma_{\text{Ext}}$	$1.53^{+0.33}_{-0.03(*)}$	$1.50^{+0.34}_{-0.00(*)}$	
		(24)	$K_{\text{Ext}}$	$2.31^{+0.38}_{-0.34}$	$2.30^{+0.38}_{-0.32}$	$10^{-5} \text{ keV}^{-1} \text{ cm}^{-2} \text{ s}^{-1}$
	const0	(25)	$C_{\text{Chandra}}$	1.09 (fixed)	1.09 (fixed)	
		(26)	$C_{\text{XMM}}$	0.89 (fixed)	0.89 (fixed)	
		(27)	$C_{\text{Swift/BAT}}$	1.00 (fixed)	1.00 (fixed)	
		$\chi^2/\text{dof} (\chi_r^2)$	649.0/618 (1.05)	644.7/618 (1.04)		

NOTE— (1) Hydrogen column density of warm absorbers at the epoch of the Chandra and XMM-Newton observation, respectively. (2) Logarithmic ionization parameter,  $\xi$  ( $\text{erg cm s}^{-1}$ ) of warm absorbers at the epoch of the Chandra and XMM-Newton observation, respectively. (3) Power-law photon index of the direct component. (4) Power-law normalization at 1 keV. (5) Normalization of the RELXILL model. (6) The reflection strength of the pexrav model (the solid angle of the reflector normalized by  $2\pi$ ). (7) Normalization of the zgauss model. (8) Hydrogen column density along the equatorial plane of the XCLUMPY torus model. (9) Torus angular width. (10) Normalization of the apec model. (11) Temperature of the apec model. (12)–(14) Time variability constant of Chandra, XMM-Newton, and Swift/BAT relative to NuSTAR, respectively. (15) Hydrogen column density along the line of sight determined by the torus parameters through Equation (5). (16) Intrinsic 2–10 keV luminosity of Mrk 739E at the epoch of the Chandra observation. (17)–(22) Parameters for Mrk 739W corresponding to (3), (4), (6), (8), (15) and (16), respectively. (23) Power-law photon index of the extended emission. (24) Power-law normalization at 1 keV. (25)–(27) Cross-calibration constant of Chandra, XMM-Newton, and Swift/BAT relative to NuSTAR, respectively.

\*The parameter reaches a limit of its allowed range.

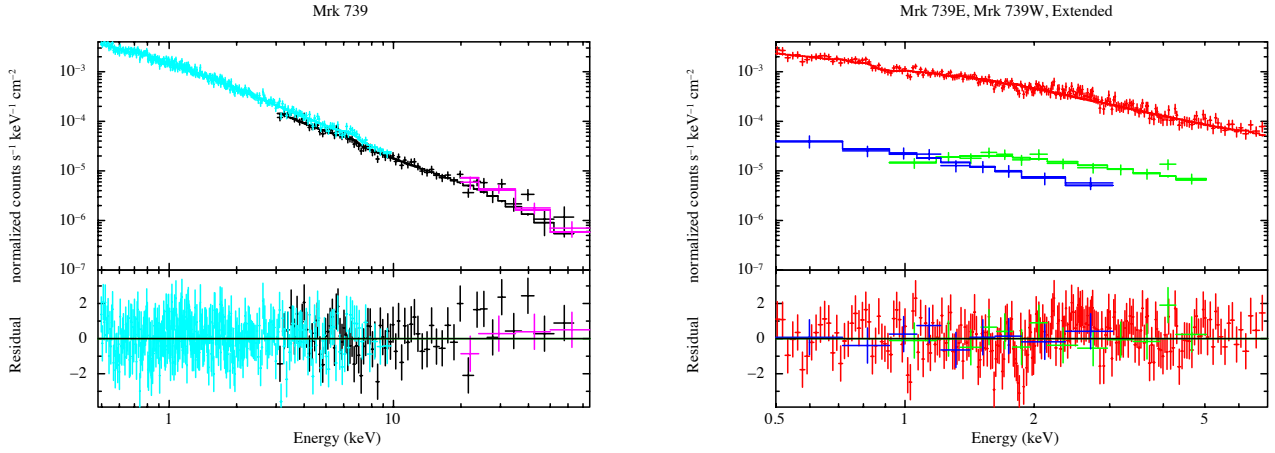


**Figure 2.** The observed spectra of Mrk 739 folded with the energy responses but corrected for the effective area (crosses). The best-fit models are overplotted (lines). (Left) The black, light blue, and magenta crosses and lines represent the NuSTAR, XMM-Newton, and Swift/BAT data of the total spectrum of Mrk 739, respectively. (Right) The red, green, and blue crosses and lines represent the Chandra spectra of Mrk 739E, Mrk 739W, and the extended emission, respectively. The residuals are plotted in the lower panels.

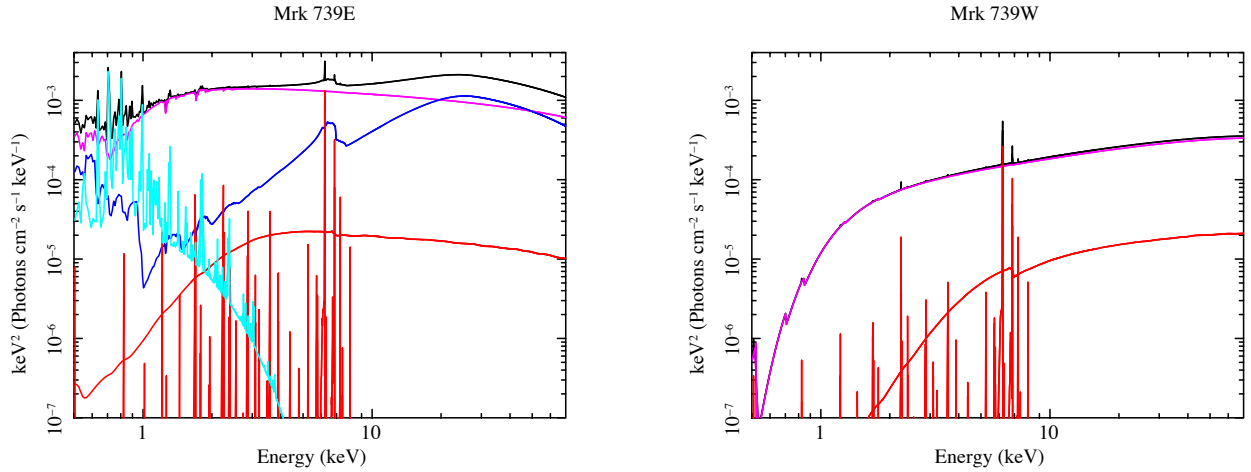


**Figure 3.** The best-fit models in units of  $E I_E$ , where  $I_E$  is the energy flux at the energy  $E$ . The black, magenta, red, blue, and cyan lines represent the total model, direct component, reflection component from the torus, reflection component from the accretion disk, and optically-thin thermal emission, respectively. (Left) The best-fit model of Mrk 739E at the epoch of the Chandra observation. (Right) The best-fit model of Mrk 739W.

**Table 3.** Best-fit torus parameters of Mrk 739E

$\sigma$ (degree)	$N_{\text{H}}^{\text{Equ}}(10^{23} \text{ cm}^{-2})$	$\chi^2/\text{dof} (\chi_r^2)$
10	$100_{-99.0(*)}^{+0.00(*)}$	644.0/618(1.04)
15	$1.00_{-0.00(*)}^{+4.30}$	644.7/618(1.04)
20	$1.00_{-0.00(*)}^{+0.21}$	654.6/618(1.06)

NOTE—  $\sigma$  is a fixed value, while  $N_{\text{H}}^{\text{Equ}}$  is a free parameter.

\*The parameter reaches a limit of its allowed range.

et al. (2021) find that AGNs in late-merger U/LIRGs show  $C_{\text{T}}^{(22)} = 0.71 \pm 0.16$  (mean and standard deviation) at  $\log \lambda_{\text{Edd}} > -1.5$ , which is significantly larger than those of normal AGNs at the same Eddington ratios (see also Yamada et al. 2020). This implies that the AGNs in late mergers have distinct structures from normal AGNs, possibly affected by the merger-driven quasi-spherical mass outflow and resultant enhanced outflow (see Figure 13 of Yamada et al. 2021). Other recent studies also point towards a larger obscuration of AGNs in dual galaxy systems. De Rosa et al. (2018) study X-ray absorption properties of four dual systems with projected separations of 30 – 60 kpc, and find that the fraction of obscured ( $\log N_{\text{H}}/\text{cm}^{-2} > 22$ ) AGNs,  $84 \pm 4$  %, is higher than that of isolated AGNs detected with Swift/BAT ( $46 \pm 3$  %; Ricci et al. 2015). Guainazzi et al. (2021) investigate the X-ray properties of 32 galaxy pairs with projected separations of  $\leq 150$  kpc and find that AGNs in galaxy pairs tend to be obscured (a fraction of  $> 70$ %).

Using the torus parameters ( $\sigma$  and  $N_{\text{H}}^{\text{Equ}}$ ) of XCLUMPY, we calculate  $C_{\text{T}}^{(22)}$  as follows (see also Equation (6) in Ogawa et al. 2021). Here, we define the critical elevation angle  $\theta_c$ , which satisfies  $N_{\text{H}}^{\text{LOS}}(\theta_c) = 10^{22}$  in the Equation (5). Then,  $C_{\text{T}}^{(22)}$  can be calculated as follows:

$$\begin{aligned}
 C_{\text{T}}^{(22)} &= \frac{1}{4\pi} \int_0^{2\pi} \int_{\frac{\pi}{2}-\theta_c}^{\frac{\pi}{2}+\theta_c} \sin \theta d\theta d\phi \\
 &= \sin \left( \sigma \sqrt{\ln \left( \frac{N_{\text{H}}^{\text{Equ}}}{10^{22} \text{ cm}^{-2}} \right)} \right) \quad (7)
 \end{aligned}$$

Since we are not able to determine  $N_{\text{H}}^{\text{Equ}}$  and  $\sigma$  simultaneously due to their parameter coupling, we estimate  $N_{\text{H}}^{\text{Equ}}$  for the three cases,  $\sigma = 10^\circ$ ,  $15^\circ$ , or  $20^\circ$  (see Section 3.1). We find that  $C_{\text{T}}^{(22)}$  of Mrk 739E is smaller than 0.50 at a 90% confidence limit for any values of  $\sigma$  we adopted.

In the Figure 4, the relation between  $C_{\text{T}}^{(22)}$  and  $\lambda_{\text{Edd}}$  obtained by Ricci et al. (2017b) for local hard X-ray selected AGNs, which are typically found in nonmerging galaxies, is shown. The points correspond to Mrk 739E (red) and the late-merger U/LIRGs (cyan; Yamada et al. 2021). The  $C_{\text{T}}^{(22)}$  values of the late-merger U/LIRGs are calculated from the XCLUMPY parameters in the same manner as in this paper. Here, the Eddington ratio of Mrk 739E ( $\log \lambda_{\text{Edd}} = -0.15$ ) is calculated from the bolometric luminosity based on the UV data (Koss et al. 2011),  $L_{\text{bol}} = 1.0 \times 10^{45} \text{ erg s}^{-1}$ , and the black hole mass estimated by Koss et al. (2011),  $\log M_{\text{BH}}/M_{\odot} \sim 7.04$ .

Figure 4 shows that the AGN torus of Mrk 739E has a smaller covering fraction than those of the late-merger U/LIRGs. Interestingly, the covering fraction is consistent with those of nonmergers at the same Eddington ratios. To verify the statistical significance of this result, we conduct Monte Carlo simulations with a sample size of  $10^6$  by assuming that the intrinsic values of  $C_{\text{T}}^{(22)}$  follow a gaussian distribution with a mean of 0.71 and a standard deviation of 0.16, the distribution of the late-merger U/LIRGs. Additionally, we assume that  $C_{\text{T}}^{(22)}$  varies from its intrinsic value with a standard deviation of 0.07, the 1- $\sigma$  error obtained by our analysis. We find that the probability of having  $C_{\text{T}}^{(22)}$  smaller than 0.39, the best fit value of our analysis, is 3.5%. We thus suggest that the AGN torus of Mrk 739E has a smaller covering fraction than those of the late-merger U/LIRGs at a  $>95$ % confidence level. Accordingly, we suggest that Mrk 739E is an exception to the idea that dual systems generally show large obscurations (e.g., De Rosa et al. 2018, Guainazzi et al. 2021). The bolometric to 2–10 keV luminosity correction factor of Mrk 739E is calculated to be  $\kappa_{2-10} \sim 90$  (based on the Chandra spectrum). Considering the fact that Mrk 739E has a high Eddington ratio ( $\log \lambda_{\text{Edd}} = -0.15$ ), this  $\kappa_{2-10}$  value is consistent with typical values of local hard X-ray selected AGNs at similar Eddington ratios, which show higher bolometric correction factors compared with those of AGNs at lower Eddington ratios ( $\kappa_{2-10} \sim 20$  at  $\log \lambda_{\text{Edd}} < -1.0$ , see e.g., Vasudevan & Fabian 2007; Lusso et al. 2012). However, it is much smaller than those found for the late-merger U/LIRGs ( $\kappa_{2-10} \sim 1000$ ; Yamada et al. 2021). This also supports the idea that the AGN in Mrk 739E is just neither deeply buried nor X-ray weak, even though it is in a late merger.

The difference in the AGN structure between Mrk 739E and late-merger U/LIRGs may be explained by considering the properties of its host galaxy. The stellar mass of Mrk 739E is estimated to be  $\log M_{\text{stellar}}/M_{\odot} \sim 10.86$  based on the K-band lumi-

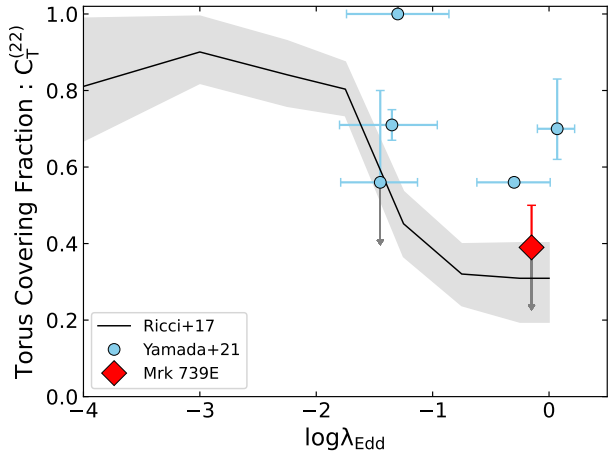


**Figure 4.** Relationship between  $\lambda_{\text{Edd}}$  and  $C_T^{(22)}$  for Swift/BAT selected AGNs (black line) and  $1\sigma$  uncertainties (the gray shaded areas) obtained by Ricci et al. (2017b). Our result for Mrk 739E (red diamond; the best-fit value obtained for  $\sigma = 15^\circ$  is adopted) and those for the late-merger U/LIRGs (cyan circles; Yamada et al. 2021) are overplotted. The arrows represent the results reaching the lower boundary.

nosity excluding the AGN region (Tubín et al. 2021). Using the far-infrared luminosity of the total Mrk 739 system, the SFR of Mrk 739E is constrained to be lower than  $6.9 M_\odot \text{ yr}^{-1}$ , which includes the contribution from Mrk 739W. These  $M_{\text{stellar}}$  and SFR values locates Mrk 739E as a main sequence star-forming galaxy or a star-formation quenching galaxy (Tubín et al. 2021), in contrast to the late-merger U/LIRGs, which are mostly star burst galaxies (e.g., Shangguan et al. 2019; Yamada et al. 2021). Assuming that the SFR is proportional to the 1.4th power of gas mass (Schmidt 1959),  $\sim 10$  times smaller SFR- $M_{\text{stellar}}$  ratio of Mrk 739E means that it has a  $\sim 0.2$  times smaller gas-to-stellar mass ratio compared with the late-merger U/LIRGs. Thus, our results suggest that the gas-to-mass ratio of the host galaxy is an important parameter to determine the circumnuclear environment of an AGN in a late merger. In fact, recent numerical simulations of galaxy mergers show that both SFR and nuclear obscuration (in terms of column density) become weaker in gas-poor mergers than in gas-rich ones (Blecha et al. 2018). Our results are consistent with this picture.

## 5. CONCLUSION

In this paper, we have reported the results of broadband X-ray spectral (0.5–70 keV) analysis of the dual-AGN system Mrk 739, utilizing currently the highest-quality data observed with NuSTAR, Chandra, XMM-Newton and Swift/BAT. The latest X-ray clumpy torus

model, XCLUMPY (Tanimoto et al. 2019), has been applied. Our main conclusions are summarized below.

1. The X-ray spectrum of Mrk 739E is well reproduced by a direct power-law component and its reflection components from the accretion disk (RELXILL) and the torus (XCLUMPY). Time-variable warm absorbers are detected. The X-ray spectrum of Mrk 739W can be modelled by an absorbed power-law and its reflection from the torus.
2. We have estimated the line of sight column densities by cold matter to be  $N_{\text{H}} < 6.5 \times 10^{19} \text{ cm}^{-2}$  and  $N_{\text{H}} = 6.9^{+3.2}_{-1.7} \times 10^{21} \text{ cm}^{-2}$  and the intrinsic X-ray luminosities to be  $1.0 \times 10^{43}$  and  $7.5 \times 10^{41} \text{ erg s}^{-1}$  for Mrk 739E and Mrk 739W, respectively. This confirms that Mrk 739E is an unabsorbed moderately-luminous AGN, whereas Mrk 739W is a weakly absorbed, low-luminosity AGN.
3. On the basis of the parameters of XCLUMPY, we have determined the torus covering fraction of Mrk 739E to be  $C_T^{(22)} < 0.50$ . This is smaller than those of local late-merger U/LIRGs at similar Eddington rates,  $C_T^{(22)} = 0.71 \pm 0.16$  (mean and standard deviation; Yamada et al. 2021).
4. Our result is a counterexample against the idea that AGNs are always deeply buried by gas and dust (i.e., the AGN tori have large covering fractions) in the late-stage mergers. We suggest that the gas-to-mass ratio of the host galaxy is an important parameter to determine the circumnuclear environment, which is consistent with recent numerical simulations of galaxy mergers. Further studies based on a larger sample of this type of AGNs are required to confirm this conclusion.

This work has been financially supported by the Grant-in-Aid for JSPS Research Fellowships 19J22216, 22K20391 (S.Y.), 20J00119 (A.T.), 21J13894 (S.O.), and for Scientific Research 20H01946 (Y.U.). S.Y. is also grateful for support from RIKEN Special Postdoctoral Researcher Program. C.R. acknowledges support from the Fondecyt Iniciacion grant 11190831 and ANID BASAL project FB210003.

We have made use of NuSTAR Data Analysis Software (NuSTARDAS) jointly developed by the Space Science Data Center (SSDC; ASI, Italy) and the California Institute of Technology (USA). We have utilized data from Chandra, supported by the Chandra X-ray Observatory Center operated by the Smithsonian Astrophysical Observatory and data from XMM-Newton, an ESA science mission with instruments and contributions directly funded by ESA Member States and NASA. We also acknowledge the use of public data from the Swift data archive.

*Facilities:* NuSTAR, Chandra, XMM-Newton, Swift.

*Software:* HEASoft (v6.28; [Nasa High Energy Astrophysics Science Archive Research Center \(Heasarc\) 2014](#)), NuSTARDAS (v2.0.0), SAS (v18.0.0; [Gabriel et al. 2004](#)), CIAO (v4.12; [Fruscione et al. 2006](#)), XSPEC (v12.11.1; [Arnaud 1996](#)), XCLUMPY ([Tanimoto et al. 2019](#)), RELXILL (v1.4.0; [Dauser et al. 2013](#); [García et al. 2014](#)).

## REFERENCES

- Anders, E., & Grevesse, N. 1989, *GeoCoA*, 53, 197, doi: [10.1016/0016-7037\(89\)90286-X](https://doi.org/10.1016/0016-7037(89)90286-X)
- Arnaud, K. A. 1996, in *Astronomical Society of the Pacific Conference Series*, Vol. 101, *Astronomical Data Analysis Software and Systems V*, ed. G. H. Jacoby & J. Barnes, 17
- Bautista, M. A., & Kallman, T. R. 2001, *ApJS*, 134, 139, doi: [10.1086/320363](https://doi.org/10.1086/320363)
- Blecha, L., Snyder, G. F., Satyapal, S., & Ellison, S. L. 2018, *MNRAS*, 478, 3056, doi: [10.1093/mnras/sty1274](https://doi.org/10.1093/mnras/sty1274)
- Dauser, T., Garcia, J., Wilms, J., et al. 2013, *Monthly Notices of the Royal Astronomical Society*, 430, 1694–1708, doi: [10.1093/mnras/sts710](https://doi.org/10.1093/mnras/sts710)
- Dauser, T., Wilms, J., Reynolds, C. S., & Brenneman, L. W. 2010, *Monthly Notices of the Royal Astronomical Society*, 409, 1534–1540, doi: [10.1111/j.1365-2966.2010.17393.x](https://doi.org/10.1111/j.1365-2966.2010.17393.x)
- De Rosa, A., Vignali, C., Husemann, B., et al. 2018, *MNRAS*, 480, 1639, doi: [10.1093/mnras/sty1867](https://doi.org/10.1093/mnras/sty1867)
- Ferrarese, L., & Merritt, D. 2000, *ApJL*, 539, L9, doi: [10.1086/312838](https://doi.org/10.1086/312838)
- Fruscione, A., McDowell, J. C., Allen, G. E., et al. 2006, in *Society of Photo-Optical Instrumentation Engineers (SPIE) Conference Series*, Vol. 6270, *Society of Photo-Optical Instrumentation Engineers (SPIE) Conference Series*, ed. D. R. Silva & R. E. Doxsey, 62701V, doi: [10.1117/12.671760](https://doi.org/10.1117/12.671760)
- Gabriel, C., Denby, M., Fyfe, D. J., et al. 2004, in *Astronomical Society of the Pacific Conference Series*, Vol. 314, *Astronomical Data Analysis Software and Systems (ADASS) XIII*, ed. F. Ochenbein, M. G. Allen, & D. Egret, 759
- García, J., Dauser, T., Lohfink, A., et al. 2014, *The Astrophysical Journal*, 782, 76, doi: [10.1088/0004-637x/782/2/76](https://doi.org/10.1088/0004-637x/782/2/76)

- Garmire, G. P., Bautz, M. W., Ford, P. G., Nousek, J. A., & Ricker, George R., J. 2003, in *Society of Photo-Optical Instrumentation Engineers (SPIE) Conference Series*, Vol. 4851, X-Ray and Gamma-Ray Telescopes and Instruments for Astronomy., ed. J. E. Truemper & H. D. Tananbaum, 28–44, doi: [10.1117/12.461599](https://doi.org/10.1117/12.461599)
- Gehrels, N., Chincarini, G., Giommi, P., et al. 2004, *ApJ*, 611, 1005, doi: [10.1086/422091](https://doi.org/10.1086/422091)
- Guainazzi, M., De Rosa, A., Bianchi, S., et al. 2021, *MNRAS*, 504, 393, doi: [10.1093/mnras/stab808](https://doi.org/10.1093/mnras/stab808)
- Harrison, F. A., Craig, W. W., Christensen, F. E., et al. 2013, *The Astrophysical Journal*, 770, 103, doi: [10.1088/0004-637x/770/2/103](https://doi.org/10.1088/0004-637x/770/2/103)
- Hopkins, P. F., Hernquist, L., Cox, T. J., & Kereš, D. 2008, *The Astrophysical Journal Supplement Series*, 175, 356–389, doi: [10.1086/524362](https://doi.org/10.1086/524362)
- Hopkins, P. F., Somerville, R. S., Hernquist, L., et al. 2006, *ApJ*, 652, 864, doi: [10.1086/508503](https://doi.org/10.1086/508503)
- Imanishi, M., Dudley, C. C., & Maloney, P. R. 2006, *ApJ*, 637, 114, doi: [10.1086/498391](https://doi.org/10.1086/498391)
- Imanishi, M., Nakagawa, T., Ohyama, Y., et al. 2008, *PASJ*, 60, S489, doi: [10.1093/pasj/60.sp2.S489](https://doi.org/10.1093/pasj/60.sp2.S489)
- Imanishi, M., & Saito, Y. 2014, *ApJ*, 780, 106, doi: [10.1088/0004-637X/780/1/106](https://doi.org/10.1088/0004-637X/780/1/106)
- Jansen, F., Lumb, D., Altieri, B., et al. 2001, *A&A*, 365, L1, doi: [10.1051/0004-6361:20000036](https://doi.org/10.1051/0004-6361:20000036)
- Kallman, T., & Bautista, M. 2001, *ApJS*, 133, 221, doi: [10.1086/319184](https://doi.org/10.1086/319184)
- Kawaguchi, T., Yutani, N., & Wada, K. 2020, *ApJ*, 890, 125, doi: [10.3847/1538-4357/ab655a](https://doi.org/10.3847/1538-4357/ab655a)
- Kawamuro, T., Ueda, Y., Tazaki, F., Ricci, C., & Terashima, Y. 2016, *ApJS*, 225, 14, doi: [10.3847/0067-0049/225/1/14](https://doi.org/10.3847/0067-0049/225/1/14)
- Kormendy, J., & Ho, L. C. 2013, *Annual Review of Astronomy and Astrophysics*, 51, 511–653, doi: [10.1146/annurev-astro-082708-101811](https://doi.org/10.1146/annurev-astro-082708-101811)
- Koss, M., Mushotzky, R., Treister, E., et al. 2012, *The Astrophysical Journal*, 746, L22, doi: [10.1088/2041-8205/746/2/L22](https://doi.org/10.1088/2041-8205/746/2/L22)
- Koss, M., Mushotzky, R., Veilleux, S., et al. 2011, *The Astrophysical Journal*, 735, L42, doi: [10.1088/2041-8205/735/2/L42](https://doi.org/10.1088/2041-8205/735/2/L42)
- Lusso, E., Comastri, A., Simmons, B. D., et al. 2012, *MNRAS*, 425, 623, doi: [10.1111/j.1365-2966.2012.21513.x](https://doi.org/10.1111/j.1365-2966.2012.21513.x)
- Madsen, K. K., Beardmore, A. P., Forster, K., et al. 2017, *AJ*, 153, 2, doi: [10.3847/1538-3881/153/1/2](https://doi.org/10.3847/1538-3881/153/1/2)
- Magdziarz, P., & Zdziarski, A. A. 1995, *MNRAS*, 273, 837, doi: [10.1093/mnras/273.3.837](https://doi.org/10.1093/mnras/273.3.837)
- Magorrian, J., Tremaine, S., Richstone, D., et al. 1998, *AJ*, 115, 2285, doi: [10.1086/300353](https://doi.org/10.1086/300353)
- Nandra, K., O’Neill, P. M., George, I. M., & Reeves, J. N. 2007, *MNRAS*, 382, 194, doi: [10.1111/j.1365-2966.2007.12331.x](https://doi.org/10.1111/j.1365-2966.2007.12331.x)
- Nasa High Energy Astrophysics Science Archive Research Center (Heasarc). 2014, HEASoft: Unified Release of FTOOLS and XANADU, Astrophysics Source Code Library, record ascl:1408.004. <http://ascl.net/1408.004>
- Netzer, H., Kollatschny, W., & Fricke, K. J. 1987, *A&A*, 171, 41
- Ogawa, S., Ueda, Y., Tanimoto, A., & Yamada, S. 2021, *ApJ*, 906, 84, doi: [10.3847/1538-4357/abccce](https://doi.org/10.3847/1538-4357/abccce)
- Ogawa, S., Ueda, Y., Yamada, S., Tanimoto, A., & Kawaguchi, T. 2019, *ApJ*, 875, 115, doi: [10.3847/1538-4357/ab0e08](https://doi.org/10.3847/1538-4357/ab0e08)
- Oh, K., Koss, M., Markwardt, C. B., et al. 2018, *ApJS*, 235, 4, doi: [10.3847/1538-4365/aaa7fd](https://doi.org/10.3847/1538-4365/aaa7fd)
- Patrick, A. R., Reeves, J. N., Porquet, D., et al. 2012, *MNRAS*, 426, 2522, doi: [10.1111/j.1365-2966.2012.21868.x](https://doi.org/10.1111/j.1365-2966.2012.21868.x)
- Ramos Almeida, C., & Ricci, C. 2017, *Nature Astronomy*, 1, 679, doi: [10.1038/s41550-017-0232-z](https://doi.org/10.1038/s41550-017-0232-z)
- Ricci, C., Ueda, Y., Koss, M. J., et al. 2015, *ApJL*, 815, L13, doi: [10.1088/2041-8205/815/1/L13](https://doi.org/10.1088/2041-8205/815/1/L13)
- Ricci, C., Bauer, F. E., Treister, E., et al. 2017a, *MNRAS*, 468, 1273, doi: [10.1093/mnras/stx173](https://doi.org/10.1093/mnras/stx173)
- Ricci, C., Trakhtenbrot, B., Koss, M. J., et al. 2017b, *Nature*, 549, 488, doi: [10.1038/nature23906](https://doi.org/10.1038/nature23906)
- Ricci, C., Ho, L. C., Fabian, A. C., et al. 2018, *MNRAS*, 480, 1819, doi: [10.1093/mnras/sty1879](https://doi.org/10.1093/mnras/sty1879)
- Ricci, C., Privon, G. C., Pfeifle, R. W., et al. 2021, *MNRAS*, 506, 5935, doi: [10.1093/mnras/stab2052](https://doi.org/10.1093/mnras/stab2052)
- Ricci, C., Ananna, T. T., Temple, M. J., et al. 2022, *arXiv e-prints*, arXiv:2209.00014. <https://arxiv.org/abs/2209.00014>
- Sanders, D. B., & Mirabel, I. F. 1996, *ARA&A*, 34, 749, doi: [10.1146/annurev.astro.34.1.749](https://doi.org/10.1146/annurev.astro.34.1.749)
- Schmidt, M. 1959, *ApJ*, 129, 243, doi: [10.1086/146614](https://doi.org/10.1086/146614)
- Shangguan, J., Ho, L. C., Li, R., et al. 2019, *ApJ*, 870, 104, doi: [10.3847/1538-4357/aaf21a](https://doi.org/10.3847/1538-4357/aaf21a)
- Stierwalt, S., Armus, L., Surace, J. A., et al. 2013, *ApJS*, 206, 1, doi: [10.1088/0067-0049/206/1/1](https://doi.org/10.1088/0067-0049/206/1/1)
- Strüder, L., Briel, U., Dennerl, K., et al. 2001, *A&A*, 365, L18, doi: [10.1051/0004-6361:20000066](https://doi.org/10.1051/0004-6361:20000066)
- Tanimoto, A., Ueda, Y., Odaka, H., et al. 2019, *The Astrophysical Journal*, 877, 95, doi: [10.3847/1538-4357/ab1b20](https://doi.org/10.3847/1538-4357/ab1b20)
- Tanimoto, A., Ueda, Y., Odaka, H., et al. 2020, *ApJ*, 897, 2, doi: [10.3847/1538-4357/ab96bc](https://doi.org/10.3847/1538-4357/ab96bc)
- Tanimoto, A., Ueda, Y., Odaka, H., Yamada, S., & Ricci, C. 2022, *ApJS*, 260, 30, doi: [10.3847/1538-4365/ac5f59](https://doi.org/10.3847/1538-4365/ac5f59)

- Toba, Y., Yamada, S., Ueda, Y., et al. 2020, *ApJ*, 888, 8, doi: [10.3847/1538-4357/ab5718](https://doi.org/10.3847/1538-4357/ab5718)
- Tubín, D., Treister, E., D’Ago, G., et al. 2021, *The Astrophysical Journal*, 911, 100, doi: [10.3847/1538-4357/abedba](https://doi.org/10.3847/1538-4357/abedba)
- Uematsu, R., Ueda, Y., Tanimoto, A., et al. 2021, *ApJ*, 913, 17, doi: [10.3847/1538-4357/abf0a2](https://doi.org/10.3847/1538-4357/abf0a2)
- Urry, C. M., & Padovani, P. 1995, *PASP*, 107, 803, doi: [10.1086/133630](https://doi.org/10.1086/133630)
- Vasudevan, R. V., & Fabian, A. C. 2007, *MNRAS*, 381, 1235, doi: [10.1111/j.1365-2966.2007.12328.x](https://doi.org/10.1111/j.1365-2966.2007.12328.x)
- Weisskopf, M. C., Brinkman, B., Canizares, C., et al. 2002, *Publications of the Astronomical Society of the Pacific*, 114, 1–24, doi: [10.1086/338108](https://doi.org/10.1086/338108)
- Willingale, R., Starling, R. L. C., Beardmore, A. P., Tanvir, N. R., & O’Brien, P. T. 2013, *MNRAS*, 431, 394, doi: [10.1093/mnras/stt175](https://doi.org/10.1093/mnras/stt175)
- Yamada, S., Ueda, Y., Oda, S., et al. 2018, *The Astrophysical Journal*, 858, 106, doi: [10.3847/1538-4357/aabacb](https://doi.org/10.3847/1538-4357/aabacb)
- Yamada, S., Ueda, Y., Tanimoto, A., et al. 2021, *ApJS*, 257, 61, doi: [10.3847/1538-4365/ac17f5](https://doi.org/10.3847/1538-4365/ac17f5)
- . 2019, *ApJ*, 876, 96, doi: [10.3847/1538-4357/ab14f0](https://doi.org/10.3847/1538-4357/ab14f0)
- . 2020, *ApJ*, 897, 107, doi: [10.3847/1538-4357/ab94b1](https://doi.org/10.3847/1538-4357/ab94b1)